AFRL-SR-AR-TR-05-

04-01234

0371

REPORT DOCUMENTATION PAGE

OMB No. 0704-0188

1. REPORT DATE *(DD-MM-YY)*: 5/08/05	2. REPORT TYPE Technical report (FINAL)	3. DATES COVERED *(From - To)* 9/2004-3/2005

4. TITLE AND SUBTITLE
Bio-inspired Organic/Inorganic Hybrid Electronic and Photonic Materials and Structures

5a. CONTRACT NUMBER

5b. GRANT NUMBER 01
F49620-~~98~~-1-0541

5c. PROGRAM ELEMENT NUMBER

6. AUTHOR(S)
Alex K-Y. Jen & Mehmet Sarikaya

5d. PROJECT NUMBER

5e. TASK NUMBER

5f. WORK UNIT NUMBER

7. PERFORMING ORGANIZATION NAME(S) AND ADDRESS(ES)

University of Washington

Department of Materials Science & Engineering, University of Washington
Seattle, WA 98195

8. PERFORMING ORGANIZATION REPORT

9. SPONSORING / MONITORING AGENCY NAME(S) AND ADDRESS(ES)

Dr. Charles Y-C. Lee
AFOSR
875 N. Randolph Street, Suite 325, Room 3112, Arlington, VA 22203

10. SPONSOR/MONITOR'S ACRONYM(S)

11. SPONSOR/MONITOR'S REPORT NUMBER(S)

12. DISTRIBUTION / AVAILABILITY STATEMENT

13. SUPPLEMENTARY NOTES

14. ABSTRACT

The goal of this research is to develop nano and meso-structured hybrid systems for the application in light harvesting, charge transfer and photocurrent generation with a high impact on the mission of the US Air Force. Our project is multifaceted and includes both bioinspiration and physical sciences approaches, all at the molecular and nanoscale levels. Our particular approach is creating nanohybrids of functional molecules coupled with nanostructured inorganics. One of the ways of achieving this complex but potentially highly functional system is combining biomacromolecular entities with functional inorganics and synthetic molecules.

15. SUBJECT TERMS

16. SECURITY CLASSIFICATION OF:			17. LIMITATION OF ABSTRACT	18. NUMBER OF PAGES	19a. NAME OF RESPONSIBLE PERSON: Alex K-Y. Jen
a. REPORT	b. ABSTRACT	c. THIS PAGE			19b. TELEPHONE NUMBER *(include area code)* (206) 543-2626

Standard Form 298 (Rev. 8-98)
Prescribed by ANSI Std. Z39.18

AIR FORCE OFFICE OF SCIENTIFIC RESEARCH

END-OF-THE-YEAR-REPORT

PUBLICATIONS/PATENTS/PRESENTATIONS/HONORS/STUDENTS REPORT

for

GRANT # F49620-01-1-0541

Bio-inspired Organic/Inorganic Hybrid Electronic and Photonic Materials and Structures

Alex K-Y. Jen and Mehmet Sarikaya

Department of Materials Science & Engineering

University of Washington

August 5, 2005

Program Objective:

The goal of this research is to develop nano and meso-structured hybrid systems for the application in light harvesting, charge transfer and photocurrent generation, with a high impact on the mission of the US Air Force. Our project is multifaceted and includes both bioinspiration and physical sciences approaches, all at the molecular and nanoscale levels. Our particular approach is creating nanohybrids of functional molecules coupled with nanostructured inorganics. One of the ways of achieving this complex but potentially highly functional system is combining biomacromolecular entities with functional inorganics and synthetic molecules.

Status of Effort:

We use biomolecules as templates to create ordered electron donor/acceptor assemblies for functional properties. In particular, we use proteins as molecular templates for assembling nanoparticles and functional π-conjugated molecular building blocks for nanotechnology and biotechnology applications relevant to USAF. In order to reach this goal, we address two major aspects: 1) proteins as molecular templates for assembly of or in conjunction with small inorganic particles; 2) assemblies of coplanar anthraquinonyl and anthryl moieties linked by an acetylenic unit and with an oligo(pyrrolethiophene) donors for highly efficient photocurrent generation.

Accomplishments and New Findings:

In general, our approach is multifaceted and uses several steps:

a. The bio-inspiration is based on self-assembled biomacromolecular, including proteineceous, systems, such as S-layer proteins, chaperons, DNA, or viruses. The advantage of using these is three folds: a. molecular recognition, b. self-assembly, and c. DNA-based technologies (genetic engineering).
b. We use designer proteins (either S-layer or chaperons) or their synthetic analogies, i.e., functionalized synthetic polymeric designer units (such as nm-diameter polystyrene beads) as nanoscale masks and electrochemically grow particles or rods on a selected inorganic surface. Since there are more than one type of discontinuities, i.e., such as "nano-openings" among the protein units or within proteins themselves forming the assembled nanostructured proteinaceous pattern, one can engineer several types of inorganic materials (nano-dots or nano-rods) on these structures;
c. Immobilize functional molecules onto these inorganic nano-particles or nanoroods through specific binding groups, either biological, such as GEPI, genetically engineered proteins for inorganics, or synthetic, such as thiol and phosphonic acid or engineered polypeptides;
d. Use these nanostructured inorganic/organic hybrids as platforms for demonstrating efficient photocurrent generation and feasibility of artificial photosynthesis.

Our research, in general, is a two-step process: During the first step, we use genetically engineered designer proteins capable of assembling inorganic materials into well-defined nanostructures via self- and co-assembly through their molecular recognition and assembly characteristics. And, using these highly organized nanostructures, in the second step, we hybridize functional molecular units and demonstrate light harvesting and photocurrent generation. Three unique opportunities are used in the bio-inspired approach: a. ability to assemble two different inorganic materials, for example one being a conductor (metal) and the

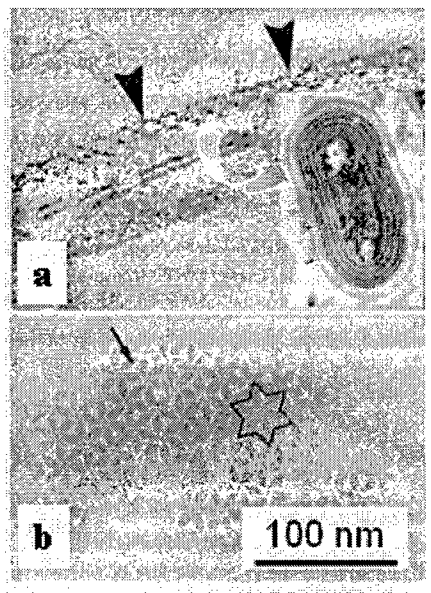

Figure 1. 2-D protein templates used for Bio-Inspiration in this proposal. (a) S-layer protein (cross-section) of a bacterium *Synechoccus* srain GL24 (inset) showing the position of the layer on the outer surface. (b) In this species, S-layer acts as a nano-template for calcite formation with nano-tiles.

other semiconductor (oxide); b. Ability to engineer and assemble/immobilize functional linkers at controlled distances; and c. Hybridization of functional molecules with biomolecules or inorganics at desired positions on a nanosubstrate for photocurrent generation. Below we give a summary of the accomplishments to date with respect to creating two-dimensional nanostructure with proteins as molecular templates. We have also demonstrated assemblies of coplanar anthraquinonyl and anthryl moieties linked by an acetylenic unit and with an oligo(pyrrolethiophene) donors and C_{60}-based dyads for highly efficient photocurrent generation.

1. Biomacromolecular Crystals as Nanomasks for Creating Ordered Functional Templates:

A. Bioinspiration: The bioinspiration is based on the formation of nano-tiles of calcite ($CaCO_3$ – rhombohedral) in some species of S-layer bacteria where the surface layer proteins act as the nanotemplate (Figure 1). Here the S-layer proteins could form all of the 17 two-dimensional space groups, from simple oblique lattice (P2) to highly symmetric hexagonal lattices (P6m).

One of the most challenging problems in nanotechnology involving small molecules and inorganic structures, such as nanowires, nanodots, and other functional units, has been organizing these nanostructures in conjunction with functional molecules at directed positions and with controlled separation and, therefore, desired number densities exceeding 10^9 units/cm^2. As shown in Figure 2, two different materials, such as metal and a semiconductor on a given substrate (metal, insulator, or another semiconductor) are organized on a surface in a long-range order forming a superlattice. Desirably, the organization should be accomplished using energy efficient processes involving, for example, self-assembly in aqueous environments. Secondly, the size of the two inorganic nanomaterials materials should be at nanometer scale (few nm

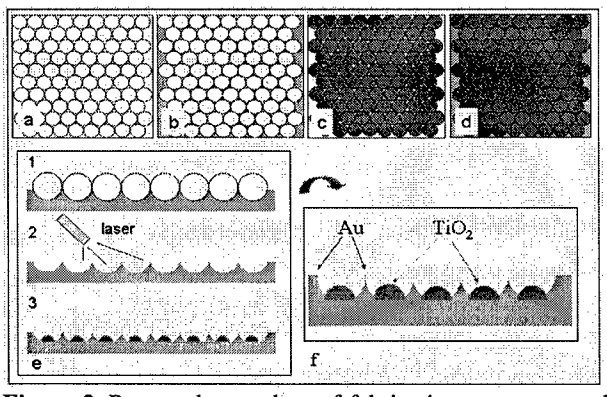

Figure 2. Proposed procedure of fabricating nanopatterned Au and TiO_2 nanoparticles using nanometer-diameter self-assembled PS spheres. (a) The original self-assembled PS spheres. (b) Formation of Au through interprotein channels. (c) Formation of TiO_2 at positions of the PS spheres after they are burned off by a laser. (d) & (f) are the final two-component (metal/semiconductor) nanostructured pattern.

diameters). And, finally, the separation should be also in the few nm-distances, and should be controlled throughout the surface. Although there are a number of newly developed nanopatterning approaches, such as μ-contact or nm-contact printing, dip-pen nanolithography, assembly of nanoparticulate or carbon nanotube systems, none of the current approaches would provide the close control necessary in the development of such a nanostructured inorganics.

B. Current Research Results:

Based on the biomimetic approach, we use biological systems as nanomask or template through which to fabricate multicomponent nanopatterned functional inorganics. We use DNA as a molecular template where a DNA-binding protein (TraI) is specifically attaches at pre-specified locations along the DNA. TraI is genetically engineered as to be fused with GEPIs (genetically engineered polypeptide for affinity to inorganic) that have been developed in our laboratories using combinatorial biology methods. We demonstrate that a GEPI, attached to DNA-binding protein and addressably located on single stranded DNA, can act as a nucleator/synthesizer as well as a molecular erector for displaying inorganic nanoparticles, metals or semiconducting oxides. We have also used S-layer as nanomask for inorganics. With which we can create nano-templated surface with both metal (a good conductor, such as Au, Ag, Pt, or Pd) and wide band-gap semiconductor oxide (e.g., TiO_2, Al_2O_3, Cu_2O, or ZnO). In the firs step, we use S-layer films from the bacterium *Deinococcus radiodurans* that can readily be placed on conducting substrates. The S-layer from this species is stripped from the surface of the bacteria and re-constituted on a selected conducting substrate used for the electrochemical growth of the inorganics.

C. Experimental Details

i. Synthesis and Directed Assembly of Inorganic Nanoparticles using GEPI attached to DNA via a designer protein, a DNA-binding protein:

Natural biomineralization processes can form equilibrium solids with compositions predicted by solution thermodynamics as well as nonequilibrium solids that are unexpected given the solution properties. Biomimetic polypeptides and RNA have shown an ability to catalyze, nucleate, and organize inorganic solids, providing control of crystal form and growth shape, but not selective growth and organization of a wholly unexpected solid composition. We demonstrate the biomimetic growth of semiconducting metal oxide Cu_2O in a chloride-based solution where Cu_2O is soluble and $Cu_2Cl(OH)_3$ is the expected solid. Nonequilibrium Cu_2O forms in the presence of an engineered variant of TraI (*E. coli* DNA helicase I) possessing a cysteine-constrained 12 amino acid Cu_2O binding polypeptide identified previously. The nucleated particles contain 2-3 nm Cu_2O cores and functional protein shells that permit assembly on DNA templates. The protein shells form and stabilize the Cu_2O nuclei because the engineered TraI variant is endowed with nanomolar surface binding affinity (K_d=1.2x10^{-8} M) that is not present in control TraI. The engineering of a protein to grow and organize a selected material under conditions where that material is nominally soluble provides new avenues for biomimetic design and synthesis of complex multimaterial inorganic structures.

Solution-based processing of inorganic materials is a highly refined art, where control of particle size, composition, and structure is guided by an understanding of electrochemical equilibria,

nucleation processes, and colloid science. However, nature's ability to select specific inorganic compositions from complex multicomponent electrolytes is largely unmatched in the laboratory. For example, marine organisms grow calcium carbonate shells from seawater supersaturated in precursor reagents (above the lysocline) whereas seawater is unsaturated in the silicic acid precursors needed to make silica. Nonetheless, silicateins and silaffins are able to grow and stabilize silica structures in seawater where they are nominally soluble, as well as catalyze silica growth under laboratory conditions. Biomimetic materials design seeks to efficiently identify biological macromolecules that can serve to nucleate, grow, and organize materials under mild ambient conditions. Combinatorial selection has emerged as an efficient means to identify inorganic synthesis moieties. Not only do these moieties catalyze nucleation and organization of the inorganics, some have also shown selectivity among alternative crystal structures and cross-binding selectivity among related inorganics. However, these inorganic synthesis moieties have not yet shown nature's ability to stabilize and build with nominally soluble solids; this trait is essential for biomimetic synthesis strategies that seek to grow complex multimaterial structures from a single pot.

Thermodynamic speciation in the $Cu–Cl^-–H_2O$ system is well established, making it a model system for exploring the selective growth of nonequilibrium solid phases (see supplementary materials). We start with a room temperature precursor solution of 6 mM cuprous chloride complex $CuCl_n^{1-n}$ (n=2 and 3) made by electrochemical oxidation of copper in 1 M NaCl electrolyte. The resulting anolyte solution, in contact with ambient air, has an oxidation-reduction potential (ORP) near 370 mV and a pH of 6.0, placing it on the thermodynamic phase boundary between the inorganic solid $Cu_2Cl(OH)_3$ and the precursor solution. The TEM micrograph in Figure 1a shows that ≈300 nm particles are present in this electrolyte and their electron diffraction pattern matches that of $Cu_2Cl(OH)_3$ as predicted by equilibrium considerations. At higher pH (>7.0), Cu_2O becomes the thermodynamically-preferred inorganic solid from $CuCl_n^{1-n}$ precursor. The pH-induced transition to Cu_2O formation is visible to the unaided eye; a yellow to red precipitate appears, depending on solution pH, with electron diffraction and Raman spectra confirming the composition (not shown). In short, our cuprous chloride complex precursor solution follows the expected thermodynamic patterns for equilibrium phase formation.

The protein TraI (DNA helicase I), an *E. coli* F plasmid-encoded protein required for bacterial conjugative DNA transfer, is used to explore the role of protein-mediated nucleation and growth from our precursor solution. This protein has two key attributes for these studies: it possesses no natural cysteine residues where thiol-mediated binding might interfere with result interpretation, and it is a DNA binding protein, which allows heirarchical assembly using DNA as a template. The experiments described here utilized two mutants of TraI, TraIi1753 and TraIi1753::CN225. TraIi1753 has a permissive insertion of 31 residues following the 1753rd residue and serves as a negative control. TraIi1753::CN225 has a dodecapeptide (RHTDGLRRIAAR) Cu_2O binding motif, denoted CN225, constrained by the formation of a disulfide bond between flanking cysteine residues, inserted within the 31 permissive residues of TraIi1753. The Cu_2O binding motif CN225 was identified using GI826 *Escherichia coli* cells harboring the FliTrx combinatorial polypeptide library (Invitrogen, Carlsbad, CA), as detailed elsewhere. Both TraI mutants are functional in conjugation, with relaxase and helicase activities.

As a control experiment, the precursor cuprous chloride solution was made in the presence of $1.2x10^{-8}$ M TraIi1753. Figure 1b shows a TEM image and electron diffraction pattern for the crystalline particles that formed. The particles are smaller (100 - 200 nm) than those formed in the absence of protein (Figure 1a), but the electron diffraction pattern shows the (201), (220), (202), (231) and (203) rings from orthorhombic $Cu_2Cl(OH)_3$ crystallites, *i.e.*, the equilibrium solid is present. Therefore, negative control TraIi1753 promotes nucleation, as most non-specific contaminants do, but it does not alter the electrochemical equilibria.

In contrast, particle formation is radically altered when the Cu_2O binding derivative TraIi1753::CN225 is introduced at a concentration of $1.2x10^{-8}$ M during the creation of precursor solution, as shown in Figure 3c. The average diameter of the particles is about 10 nm with several 100 nm clusters. Selected area electron diffraction (inset) shows concentric rings corresponding to (110), (111), (200), (211), (220) and (310) lattice planes of cubic Cu_2O. TEM imaging at higher magnification (Figure 3d) shows that the 100 nm clusters are aggregates of the smaller particles. Higher magnification images of individual nonaggregated particles (Figure 3e) suggest that each nanoparticle has a core-shell structure comprised of a dense core (about 2 nm) surrounded by a low density outer region. Convergent beam electron diffraction (Figure 3f) of a nonaggregated particle displays the {111} family of Cu_2O planes from a beam in the [110] direction. In short, a non-equilibrium solid phase, Cu_2O, has formed under the nanomolar control of an engineered protein bearing a small polypeptide insert identified using combinatorial biology techniques.

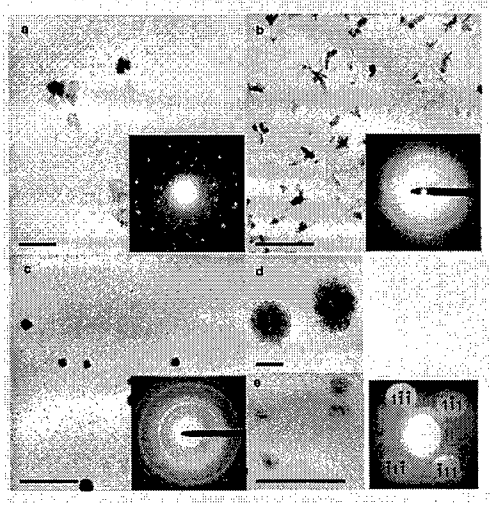

Figure 3. TEM images and selected area electron diffraction patterns of nanoparticles formed in the precursor solutions: **a**, without any protein addition; **b**, with $1.2x10^{-8}$ M TraIi1753 added as a control; and **c**, with $1.2x10^{-8}$ M TraIi1753::CN225 added. **d**, High magnification TEM image

The precursor solution hydroxide and cuprous ion concentrations are at approximately 1% of the solubility product (K_{sp}) for Cu_2O formation. Even under these thermodynamically-unfavorable conditions, a transient population of nonequilibrium solid exists, but it spontaneously redissolves since growth would increase the system free energy. To stabilize a nominally soluble species, protein must adsorb with sufficient affinity to reduce the nuclei free energy, thereby stabilizing it. Protein binding affinity for Cu_2O was quantified using an electrochemical quartz crystal microbalance with Cu_2O-coated crystals. A Cu_2O-coated crystal was incubated with 100 mM phosphate buffer for 15 mins followed by the injection of protein. Raman spectra verify that this buffer does not alter the cuprous oxide film (data not shown). Figure 4a shows the crystal resonant frequency before and after injection of $1.5x10^{-8}$ M TraIi1753 and TraIi1753::CN225. No appreciable frequency change is observed after adding the negative control TraIi1753, indicating negligible adsorption to the Cu_2O. In contrast, the Cu_2O-binding variant TraIi1753::CN225 induces a 55 Hz decline in frequency, indicating adsorption. Figure

2b shows the full concentration dependent adsorption isotherm for this protein on Cu_2O. Fitting the data to a Langmuir adsorption isotherm $\Delta f = \frac{\Delta f_{max} \times C}{K_d + C}$ yields an equilibrium dissociation constant of $K_d = 1.2\times10^{-8}$ M. Thus, it appears that high-affinity adsorption of protein on Cu_2O nuclei stabilizes them, creating particles that appear in micrographs as dense 2 nm Cu_2O cores surrounded by TraIi1753::CN225 shells. The low density protein shell is made visible in the TEM, presumably, by staining from soluble copper coordinated to protein amine groups.

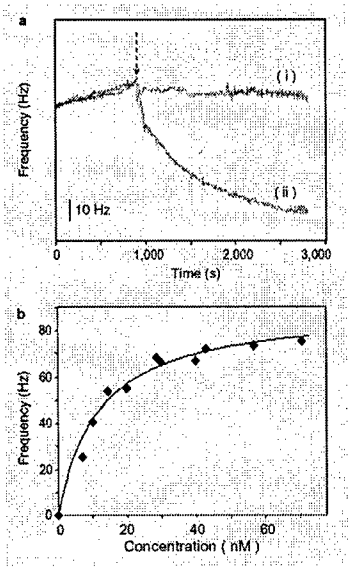

Figure 4 – Adsorption properties of TraI variants on Cu_2O measured with an electrochemical quartz crystal microbalance. A. Time course of resonance frequency with control TraIi1753 (curve i) and TraIi1753::CN225 (curve ii). The vertical arrow denotes the time where protein is added. B. Concentration dependence of resonant frequency change for traIi1753::CN225 adsorption on Cu_2O and the best fit to a Langmuir adsorption isotherm.

In vivo assays of the TraI variants show that these polypeptides are functional in conjugation, so it is likely that *in vitro* DNA binding remains intact. We mixed the core-shell Cu_2O-TraIi1753::CN225 nanoparticle solution with circular fX174 RFII DNA solution (see materials and methods) and then imaged the mixture with TEM (Figure 3). fX174 RFII DNA is the double stranded, nicked circular form of fX174 DNA. As seen in Figure 5, the protein coated Cu_2O nanoparticles self-assembled onto the DNA. Smooth-contoured nanoparticle loops are not seen in the absence of circular DNA. The fX174 RFII DNA loops are condensed to a circumference of about 400~500 nm upon adsorption of the nanoparticles, an effect that has been observed previously for other nanoparticle assembly on fX174 RFII DNA. Many individual particles can be seen as well, but the DNA itself is not visible in the TEM images.

The synthesis of inorganic materials under non-equilibrium aqueous growth conditions enables a clear path toward the creation and self-assembly of complex multimaterial systems in a single pot of electrolyte. For example, a number of research teams have identified inorganic binding peptides (IBPs) for metals, semiconductors, and insulators. Moreover, some of these IBPs are known to be portable, allowing them to be inserted into other proteins, as also demonstrated here for CN225 sequence in TraI. Thus, one can imagine generalizing the results shown here to the growth and self-assembly of multimaterial objects: A *set* of IBPs are identified that selectively bind single materials with high affinity. These IBPs are inserted into solvent-exposed permissive sites on self-organizing proteins, which are mixed into a beaker containing a stew of sub-saturated precursor salts. Because the precipitation takes place from a sub-saturated solution under protein control, the *only* precipitate to form is comprised of organized multi-material objects built from metal, semiconductor and insulator that are spatially organized with nanometer precision.

Precursor synthesis and particle formation occurred in an electrochemical cell possessing a 1 mL anolyte compartment separated from a 50 mL catholyte compartments with a glass frit.

Electrolyte consisted of 2 micron-filtered 1 M NaCl solution with or without TraIi1753 or TraIi1753::CN225 added to the anolyte. The anode and cathode were 1 cm^2 Cu foil. A Princeton Applied Research 273A Potentiostat/Galvanostat was operated galvanostatically at 10 mA for 1 min, producing approximately 6 mM total cuprous ion products. To assemble Cu_2O particles on DNA, 40 ml of anolyte solution made in the presence of $1.2x10^{-8}$ M TraIi1753::CN225 was mixed with 10 ml DNA solution ($3x10^{-8}$ M fX174 RFII DNA, circular form, diluted 10 fold from stock solution). The DNA stock solution (BioLab, New England) was 1000 μg/ml ($3x10^{-7}$ M) fX174 RFII DNA supplied in 10 mM Tris-HCl (pH 8.0) and 1 mM EDTA. TraI adsorption on Cu_2O was characterized using an electrochemical quartz crystal microbalance (EQCN-700, ELCHEMA) with 10.0 MHz AT-cut quartz crystals coated with a uniform film of electrodeposited Cu_2O. The crystals were cleaned in Piranha solution (30% H_2O_2 : 98% H_2SO_4 =1:2) prior to Cu_2O deposition.

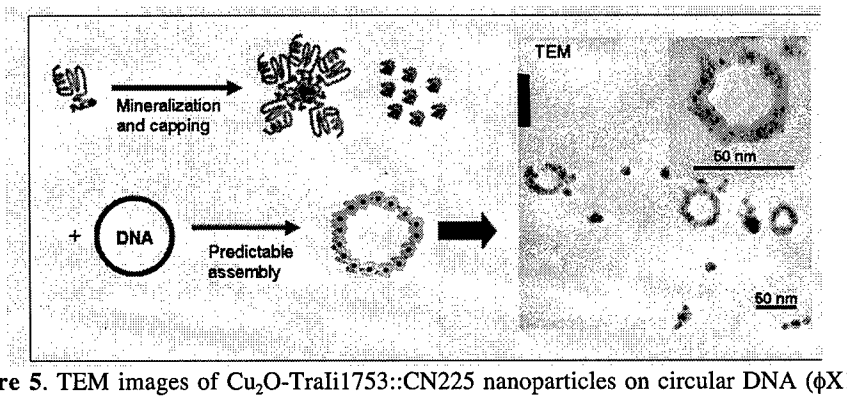

Figure 5. TEM images of Cu_2O-TraIi1753::CN225 nanoparticles on circular DNA (ϕX174 RFII DNA. 5386 base). Scale bar: 100nm.

ii. Protein immobilization on solid surfaces: Proteins were immobilized onto electrode surfaces by applying a few microliters of suspension from the stock solution (1 mg/mL protein in 5% SDS) onto electrode surfaces. For partial coverage, the droplet was immediately wicked away with a wipe leaving behind only a thin wetting aqueous film on the surface. The surface was then rinsed by repeated immersion in deionized water then air-dried. For complete coverage, a protein suspension was applied as before, with deionized water added to extend the drop to the edges of the electrode surface. This drop was allowed to dry completely, such that all suspended proteins remain on the surface. Excess detergent was removed by repeated immersion in deionized water followed by air-drying.

iii. Electrodeposition and TEM Sample Preparation: Electrodeposition experiments were performed at room temperature using a PINE 273 potentiostat in a quiescent 10 mL single compartment cell, with a platinum counter electrode and saturated calomel electrode (SCE) as reference. All electrolytes were prepared from reagent grade chemicals (Sigma and Alfa Aesar) and passed through 0.2-mm filters (Osmonics, inc.) before use. Electrodeposition times for each material presented were chosen by qualitative inspection in the TEM, with the criterion that the deposited film be near complete coverage, yet sufficiently electron transparent for electron diffraction studies. For TEM sample preparation, metallic anticapillary tweezers (DuMont) were used to make contact with the edge of a metal-coated TEM grid (the working electrode). Carefully lowering the grid at an acute angle to the electrolyte free surface, with the protein side facing the electrolyte, allowed the electrolyte meniscus to contact the protein side only.

We have developed protocols to deposit noble (Au, Pd, Pt, Ag) and non-noble metals (Cu, Ti, Al), and semiconducting oxides (Cu_2O, TiO_2, ITO, TiO_2, etc.). Here we give example of the Cu_2O deposition. Cuprous oxide (Cu_2O) plating bath was prepared following the known recipe and procedure. Briefly, the electrolyte was 0.4 M $CuSO_4$, 3.0 M lactic acid, adjusted to pH 9.0 with NaOH, and electrodeposition performed at –450 mV vs. SCE for 15 minutes.

The electrodeposition of Cu_2O through the channels in the HPI-layer protein mask produces a reasonably high fidelity hexagonal nanostructure as shown in the TEM images in Figure 4. The deposition takes place through the hydrophilic openings of the protein. Here we favor the use of TEM over AFM for imaging the electrodeposited materials because the protein is electron transparent so that, unlike in the AFM, it is removal is not necessary. In addition, electron diffraction allows the assessment of the crystallinity of the arrayed dots to be examined as well as the phase analysis. One of the reasons that we started the electrodeposition of Cu_2O, as it represents a highly functional semiconductor oxide with well-established general deposition conditions. An example of a Cu_2O film is shown in Figure 6 where the cuprous oxide was electrodeposited through the S-layer protein that was originally assembled on a thin AuPd film partially covering it with proteins. In this field of view, one can see the fine ~10-nm diameter grain structure of the Cu_2O film that, in some regions, form less ordered structure because of the lack of crystallinity of the proteins units. Back Fourier transforms of the optical transforms of the ordered regions reveal a hexagonal periodic structure. The TEM images (inset) in Figure 3 have marked similarity to the AFM images that were recorded directly from the assembled protein films themselves. The presence of regular array of cuprous oxide formation through electrodeposition as described here is a strong indication that templating by the S-layer protein film and growth through the protein channels was successful. High magnification images of these regions have proven difficult due to the background contrast of the thin metal film, so the inset in the upper left corner is an FFT-filtered (Fast Fourier Transformed) image of one of these regions. We have been also able to completely cover the surface of the AuPd substrate with a nanotemplated Cu_2O film as seen in the example. In this image one can notice that the cuprous oxide film is nanostructured with the same six-fold symmetry as single layer films throughout the observed area (in fact continuous over the entire surface the TEM sample disk of 3 mm diameter). These results demonstrates that multilayer coverage of protein does not block bottom-up filling at the electrode surface. In some regions in complete-coverage films Moiré patterns are evident. This

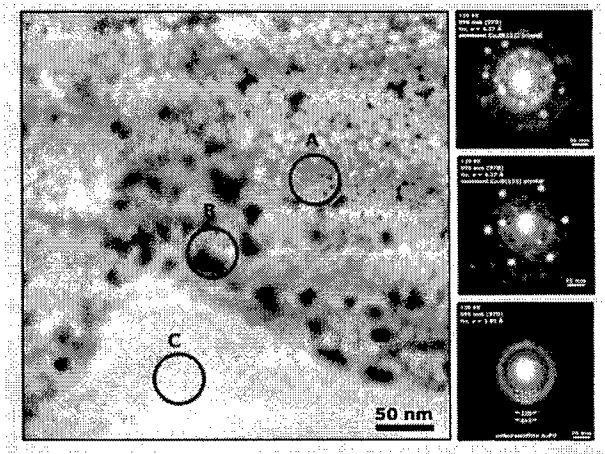

Figure 6. Transmission electron microscopy image of the ordered structure of Cu_2O (a semiconductor) on AuPd film electrodeposited through the S-layer protein as nanomask. The nanoelectron diffraction patterns on the right (from top to bottom, respectively) are from the regions indicated by A, B, and C showing face centered cubic ordering of the lattice in A and B, and no such ordering in C. Filtered image (due to student: D. Allred).

is due to electrodeposited material having grown higher than the 6-nm height of the single layer protein and, therefore, producing overlapping films of arrays corresponding to these Morié-fringed areas.

2. Assemblies of Synthetic Functional Molecules for Highly Efficient Photocurrent Generation: (A Precursor Step to Bio-inspired Full Integration of Bio and Synthetic Systems)

Inspired by very efficient conversion of solar energy into chemical potential in photosynthesis, extensive efforts have been spent to systematically organize light harvesting groups, electron donors, and electron acceptors at the molecular level to mimic the natural systems.[1] Many synthetic diads, triads and even pentads that contain porphyrins or oligothiophenes as donors and quinone, C_{60}, or peryleneimide as acceptors have been investigated for their efficiency in light-harvesting, energy transfer, electron transfer, or charge separation which are all the important processes for photosynthesis. However, it remains a very challenging task to combine all of this knowledge to create a system that can efficiently convert photons to electrons. In order to mimic the highly organized and elaborate molecular machinery of natural systems, several strategies for the construction of artificial photosynthetic systems by arranging molecules in order through lipid bilayer membranes, Langmuir-Blodgett (LB) films, or self-assembled monolayers (SAMs), have been attempted. Due to the relatively stable, uniform, well-packed and two-dimensional structures that can be formed by SAMs, a number of C_{60}-, semiconductor nanoparticle-, and metal complex-based SAMs have been explored recently and shown to exhibit promising photocurrent generation. In nature, quinone and its derivatives play a very important role as electron acceptors in photosynthetic reactions and their reversible redox behavior in solution and SAMs have also been well-studied. However, there is rarely any report regarding the use of quinone-based SAMs for photocurrent generation. In this project, we have demonstrated the design, synthesis, ordered self-assembley for efficient photocurrent generation based on an unique conjugated anthraquinone molecule.

The performance of a functionalized SAM for photocurrent generation strongly relies on its structure, order, and packing density due to the influence of unidirectional electron transfer. Therefore, it is essential to design functional molecules capable of forming well-defined and ordered self-assemblies. In our earlier work we demonstrated the use of anthrylphenylacetylene thiols to form stable and ordered self-assemblies on Au(111) surface. These molecules tend to form highly ordered two-dimensional (2D) stacked arrays through the interplay of strong π-π intermolecular stacking and chemisorptive gold-thiol interactions. Thus, by combining the electrochemically reversible properties of anthraquinone and the controllable nanoscale ordering provided by the anthrylphenylacetylene-based SAMs, we have designed and synthesized an efficient acceptor molecule, (10-(1-anthraquinonyl)acetylene)-9-anthrylmethylthiol (**1**) (Figure 7) to investigate its self-assembling characteristics and the photocurrent generation efficiency of its co-assembly with an oligo(pyrrolethiophene) donor molecule under the illumination of a monochromatic light. The anthraquinonyl moiety on top of **1** functions both as electron acceptor and a good modality for self-assembly due to its flat geometry for better π-π interactions. Because of the linear and rigid acetylene spacer, it can prevent steric hindrance between the anthraquinone moiety and the underneath anthryl group to remain co-planarity for better

conjugation. This kind of molecular arrangement will also enhance the formation of ordered SAM and facilitate vectorial electron transfer.

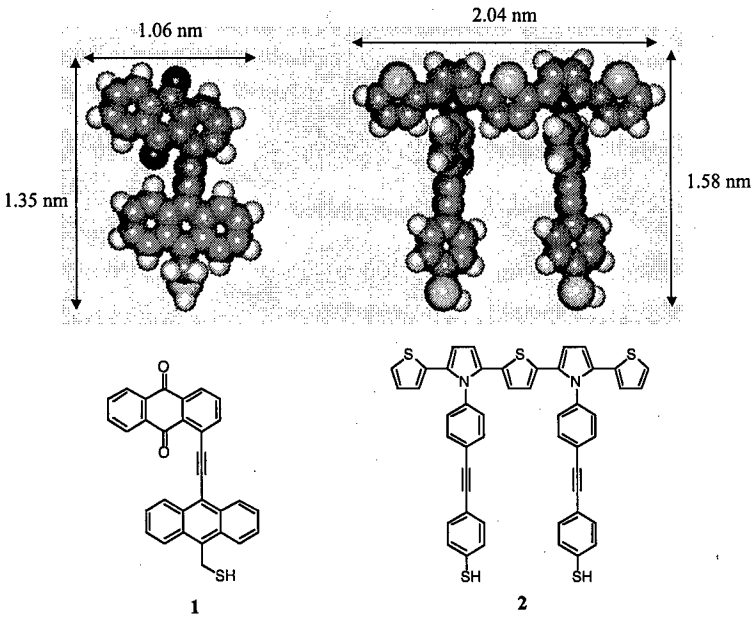

Figure 7. Schematic illustrations of self-assembling electron acceptor **1** and electron donor **2**. The structures were built by Hyperchem software and optimized by the AM1 method. The results from the AM1 calculation of molecule **1** show several kinds of stable (quasi-isoenergetic) conformations, but the molecule with a coplanar conformation forms the most stable SAM.

The SAM derived from molecule **1** was prepared by immersing Au(111)/mica substrate in a solution of **11** in EtOH at 25 °C for 24 h in the presence of ammonium hydroxide to hydrolyze the acetyl protecting group. The result from high-resolution scanning tunneling microscopy (STM) images recorded at room temperature confirms that the SAM of **1** forms a well-ordered 2D nanostructure. Figures 8a and 8b show a top view and a height-shaded surface plot, respectively. A low-pass filtered transform was employed to remove the scanning noise in the STM images. It can be seen from Figure 8a that the SAM consists of ordered bright spots with elongated features, corresponding to the individual molecules of **1**. The length of each bright spot is measured to be 0.89 ± 0.20 nm which is very close to the calculated width of molecule **1**, which indicates that these molecules stand on the Au(111) substrate through Au-S bonding. According to previous studies on self-assembly of thiols on Au(111), sulfur atoms occupy the hollow sites with lower energy compared to the bridge or top sites of Au(111). The intermolecular distance along the **A** direction is measured to be 0.61 ± 0.20 nm, which is close to 2 times that of the Au(111) lattice parameter (0.288 nm). The intermolecular distance along the **B** direction is measured to be 0.78 ± 0.20 nm, which corresponds to $\sqrt{7}$ times that of the Au(111) lattice parameter. The angle between the two directions is 42° ± 2°. Based on the intermolecular distance and orientation of molecular rows, a (2 × $\sqrt{7}$) adlayer structure for the SAM of **1** on Au(111) can be determined. A unit cell is outlined in Figure 2a. From the STM images, it can be clearly discerned that adsorbed molecules on Au(111) form a close stack with one another, similar to the interplanar stacking of graphite, with an interplanar spacing of 0.31±0.04 nm (compared to 0.34 nm for graphite). It can be attributed to the strong intermolecular π-π stacking derived from the coplanar fused rings of anthraquinone and anthrathene. The overall well-ordered and unique molecular arrangements in the SAM of **1** may also arise from a delicate interplay between the intermolecular interactions dominated by the strong intermolecular π-π

stacking, involving both steric hindrance and weak dipole-dipole interactions, and Au-S bonding between the molecules and Au(111) substrate, where the latter appears to play a secondary role.

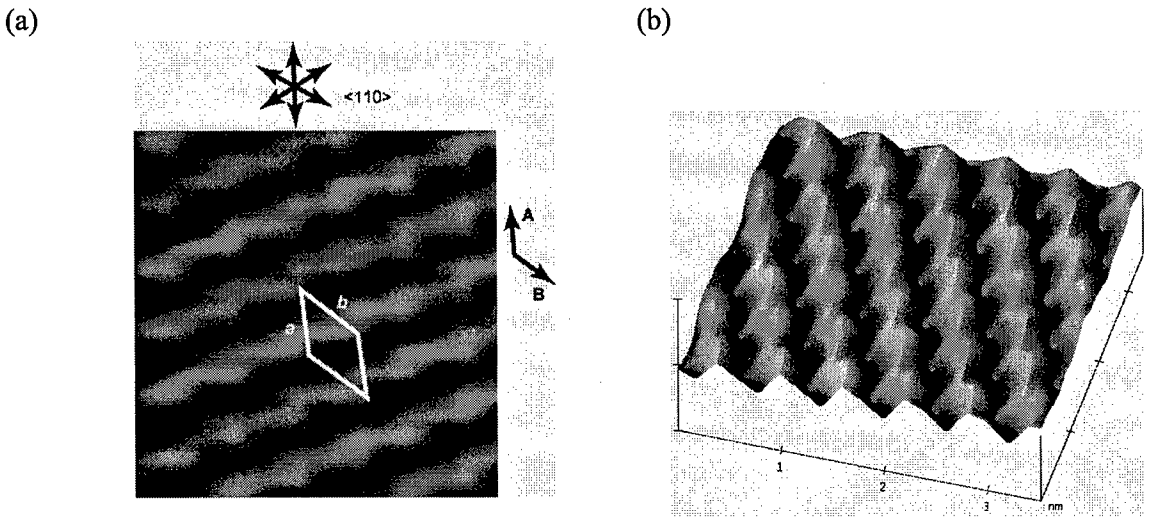

Figure 8. High-resolution STM images of ordered assemblies of electron acceptor molecule **1** on Au(111) at room temperature. (a) top-view; (b) height-shaded surface plot. Scan size is 3.5 nm × 3.5 nm. Setpoint was 500 pA, and bias was 200 mV.

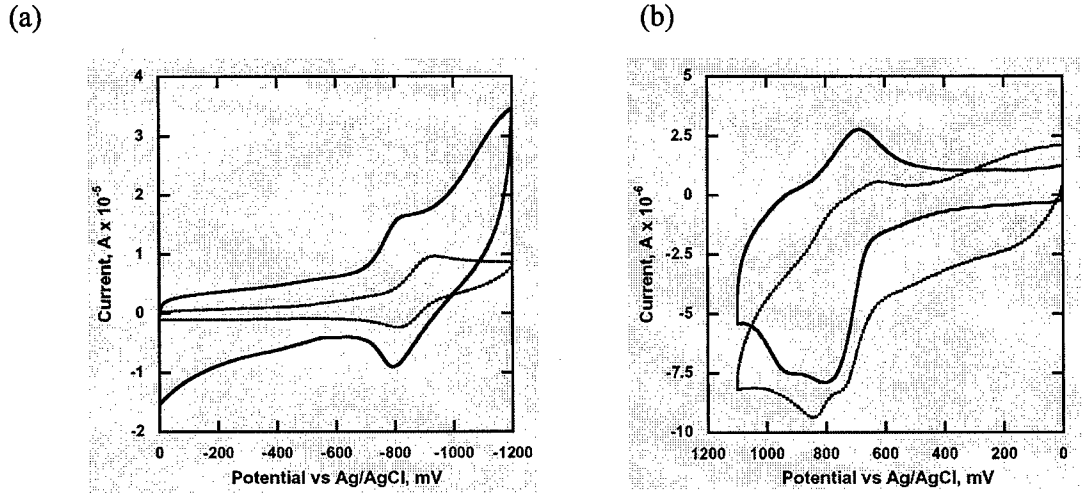

Figure 9. Cyclic voltammograms of (a) electron acceptor **1** in solution (dotted line) and its SAM on gold (solid line); (b) electron donor **2** in solution (dotted line) and its SAM on gold (solid line). Cyclic voltammograms were carried out in acetonitrile containing 0.1 M of Bu_4NPF_6 as a supporting electrolyte at a sweep rate of 100 mV/s.

The electrochemical behavior of molecules **1** and **2** as well as their SAMs on Au was evaluated by using cyclic voltammetry (CV) performed in acetonitrile containing 0.1 M of n-Bu_4NPF_6 as electrolyte and swept at a rate of 100 mV/s. The CVs of **1** and its SAM on Au showed reversible characteristics (Figure 9a) which have peak splitting of 120 mV and 30 mV, and $E_{1/2}$s of -0.87 and -0.81 V vs Ag/AgCl, respectively. The small peak-to-peak separation (30 mV) suggests

rapid electron transfer reaction kinetics for the SAM of **1** on Au. In order to construct two-component mixed SAMs for photocurrent generation efficiency studies, it is crucial to have a donor molecule that can be paired with molecule **1** for co-assembly. The molecule **2** (Figure 5) was designed to have an oligo(pyrrolethiophene) unit with lower oxidation potential than that of oligo(thiophenes), and it has two fully π-conjugated, rigid, footing thiols for better affinity to gold surface compared to the molecules with only a monothiol. The redox behavior of molecule **2** and its SAM on gold are shown in Figure 9b. Two redox-waves of **2** in solution and its SAM on gold were observed, but corresponding cathodic waves were not as clear as those anodic waves due to instability of the radical anion produced by the reduction. Redox potentials ($E_{1/2}$ vs Ag/AgCl) and peak splittings of **2** in solution and in SAM were observed to be 0.67, 0.74 V and 100 mV, 120 mV from its first oxidation step, respectively.

The amounts of adsorbed electron acceptor **1** and electron donor **2** in their homo- and co-assemblies on gold were calculated from the charge of cathodic or anodic peaks of the molecules (Table 1). The surface coverage of a homo-SAM of **1** calculated from the CV peak (4.8×10^{-10} mol/cm^2) is very close to that calculated from the STM image (5.0×10^{-10} mol/cm^2). It should be noted that the surface coverage (2.9×10^{-10} mol/cm^2) of **2** in the homo-SAM is very different from that of **1** due to the different molecular dimensions and structures, i.e. extended π-conjugation and coplanarity, which can affect intermolecular interactions and packing density of SAMs. The higher surface coverage of **1** in the homo-SAM may be due to more thermodynamically favorable packing than that of **2**, due to strong intermolecular π-π stacking and small molecular dimension. Since molecule **2** does not take part in the reduction reaction and molecule **1** does not take part in the oxidation reaction of the SAMs on gold within the scanning potential range, it can be assumed that in the CVs of mixed SAMs, the oxidation peak is derived from molecule **2** and the reduction peak is derived from molecule **1**.

The amounts of each of the self-assembled molecules on gold were systematically changed by the competitive co-adsorption onto gold surface from the solutions containing various feeding molar ratios of **1** and **2**. The surface coverage of the mixed SAMs were also calculated and listed in Table 1. As expected, the surface coverage of **2** in the mixed SAMs became higher with the increased feeding ratio of **2** in solution, while the surface coverage of **1** was smaller with the decreased feeding ratio of **1** in the solution. However, the molar ratio of **1** and **2** in the mixed SAMs do not match well with the original feeding molar ratio in the solution. The final composition of **1** and **2** in the mixed SAMs may be affected by the complicated kinetic and thermodynamic factors during the self-assembly in addition to the different concentrations of components in the feeding solution.

Table 1. Dependence of surface coverage on feeding molar ratios.

Molar ratio in solution (**2**:**1**)	Surface coverage (10^{-10} mol/cm^2)		Molar ratio in mixed SAMs[a] (**2**:**1**)
	2	**1**	
0:1	0	4.8	0:1
1:10	1.0	4.2	0.24:1
1:1	2.2	2.8	0.8:1
10:1	2.5	1.3	1.9:1
20:1	2.8	0.9	3.1:1
1:0	2.9	0	1:0

[a] Molar ratios of **2** to **1** in the mixed SAMs on the gold substrate were determined from electrochemical measurements.

The photoelectrochemical measurements were performed using the pre-assembled mixed SAMs of **1** and **2** on a gold electrode in a 0.1 M Na_2SO_4 aqueous solution containing 50 mM methyl viologen (MV^{2+}) as an electron carrier. The mixed SAM of **1** and **2** on gold was used as the working electrode, along with a platinum counter electrode and a Ag/AgCl reference electrode in a three-electrode configuration. The photocurrent was generated immediately when a monochromatic light source (360 nm) was used to illuminate the mixed SAMs in electrolyte and the initial value of photocurrent went down instantly when the illumination was terminated. As shown in Figure 10, photocurrent responses were recorded under the illumination of a monochromatic wavelength of 360 nm with 0.85 mW/cm^2 light intensity. When Au/**2**:**1** (feeding molar ratio of 10:1)/MV^{2+}/Pt was photo-irradiated under a bias voltage of –100 mV/s vs Ag/AgCl, a stable cathodic photocurrent (ca. 1425 nA/cm^2) was generated via intermolecular electron transfer from donor **2** to acceptor **1**, whereas only **1** on gold electrode showed very small photocurrent generation (less than 20 nA/cm) under the same illumination. The amount of generated photocurrent (1425 nA/cm^2) for Au/**2**:**1** (feeding molar ratio of 10:1)/MV^{2+}/Pt is comparable to the result (1700 nA/cm^2) for Au/**2**:C_{60}-anthrylphenylacetylene-thiol (feeding molar ratio of 10:1)/MV^{2+}/Pt using C_{60} as an electron acceptor. It can be seen that the mixed SAM system using anthraquinone-anthrylacetylene-thiol linked molecule **1** as an electron acceptor is quite promising to mimic the photosynthetic electron transfer of Mother Nature.

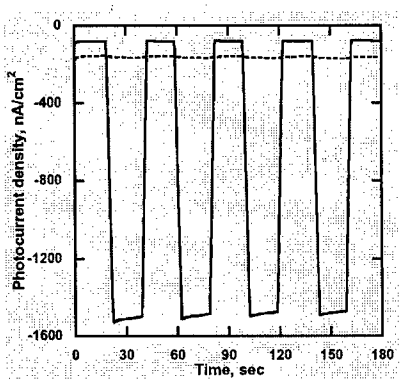

Figure 10. Photoelectrochemical response of homo-SAM of electron acceptor **1** (dotted line) and mixed SAM of **2** and **1** with a feeding molar ratio of 10:1 (solid line) on gold under illumination at 360 nm; electrolyte solution: 0.1 M Na_2SO_4 solution containing 50 mM methyl viologen (MV^{2+}) as an electron carrier; input power: 0.85 W/cm^2; applied potential: -100 mV vs Ag/AgCl.

The photocurrent generation was also investigated by varying the bias voltage to determine the direction of the current flow. Figure 8 showed the photocurrent generation in mixed SAMs upon the application of different bias potentials to the electrode. The cathodic photocurrent increases dramatically when the bias potential was applied in the range from 300 mV to –200 mV vs Ag/AgCl. The extent of change in photocurrent was larger when feeding ratio of electron donor **2** was increased in the solution. The **2:1** mixed SAM of molecule with a feeding molar ratio 10:1 showed the fastest increase in photocurrent response as a function of the bias potential. It is considered that intermolecular electron transfer in the mixed SAM of **2** and **1** (feeding molar ratio of 10:1) is more effective than those of different molar ratios. As purple bacteria, green bacteria or cyanobacteria have their own organized structures of molecular assemblies to realize highly efficient light-harvesting and photosynthesis, the optimized molecular arrangements for light absorption and electron transfer may be achieved in the mixed SAM of this pair of electron donor **2** and electron acceptor **1** with a feeding molar ratio of 10:1. The detailed feature of mixed SAMs is under investigation. The attempt to generate photocurrent with a negative bias of more than –300 mV applied to the gold electrode could not be realized due to the significant increase of the cathodic dark current. A semi-linear relationship between cathodic photocurrent vs bias potential in the presence of MV^{2+} was found; the cathodic photocurrent increased as the bias applied to the gold electrode decreased from +300 mV to –200 mV vs Ag/AgCl under the illumination of 360 nm light, demonstrating that the photocurrent flows from the gold electrode to the counter electrode through the SAM and the electrolyte. Based on its dependency on the applied bias, the photocurrent generation mechanism can be considered as follows: the photoexcitation of molecule **2** in the mixed SAMs induces intermolecular electron transfer from **2** to **1** followed by electron transfer to the redox-species ($MV^{2+}/MV^{+\cdot}$), and then the electrons are transported from $MV^{+\cdot}$ to the counter electrode (Pt) resulting in the observed cathodic photocurrent. Under a negative bias, the holes generated flow towards Au substrate to further generate cathodic photocurrent.

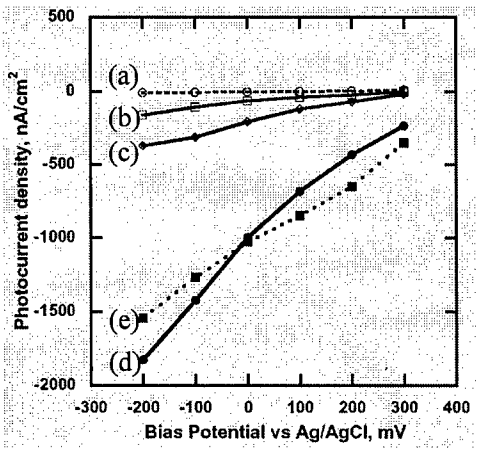

Figure 11. Photocurrent vs bias potential as a function of molar ratio of **2**:**1**; (a) 0:1; (b) 1:10; (c) 1:1; (d) 10:1; (e) 20:1; monochromic wavelength of 360 nm; electrolyte solution: 0.1 M Na_2SO_4 solution containing 50 mM methyl viologen (MV^{2+}) as an electron carrier; input power: 0.85 W/cm^2.

The action spectra of the mixed SAMs were recorded in terms of wavelength with varying molar ratios. The action spectrum of Au/**2**:**1** (feeding molar ratio of 10:1)/MV^{2+}/Pt showed a good agreement with the absorption spectrum of the mixed solution of **2** and **1** (Figure 12). When varying the excitation wavelengths within the range 360-600 nm, a maximum photocurrent was observed at 360 nm, which is close to the absorption maximum in the range of investigated wavelength.

The quantum yields were determined in terms of the feeding molar ratio by using photocurrent density, absorbance of the SAM on the electrode, and input power at the applied potential. Assuming that the absorption coefficient of **2** in a mixed SAM on gold is the same as that in solution (ε = 2.2 x 10^4 $M^{-1}cm^{-1}$ at 360 nm), the absorbance of **2** in the mixed SAMs on gold with the feeding molar ratio of 10:1 (**2**:**1**) was calculated to be 1.1 x10^{-2} at 360 nm. The quantum yield was calculated based on the assumption that the major photon absorber is electron donor **2**, not electron acceptor **1**, since the molecule **2** strongly absorbs photons at 360 nm, based on the UV spectrum. The larger quantum yields were achieved by increasing the molar ratio of **2** to **1** until reaching the highest quantum yield value at the ratio of 10:1. In order to compare our result to the reported ones in the literatures, we calculated the quantum yields of the observed cathodic photocurrent at –100 mV. The quantum yield of photocurrent generation for the mixed SAM with the feeding molar ratio of 10:1 (**2**:**1**) was determined to be 23.1 % at –100 mV vs Ag/AgCl with a monochromatic wavelength of 360 nm. The quantum yields for mixed SAMs with molar ratios of 1:10, 1:1, 10:1 and 20:1 (**2**:**1**) were 4.2, 5.5, 23.1 and 18.9 %, respectively. It should be noted that this value of quantum yield for the mixed SAM of **2** and **1** at the molar ratio of 10:1 is much larger than those in similar photoelectrochemical cells using mixed SAMs of porphyrin and alkanethiol (0.26 %), C_{60}-linked alkanethiol SAMs (7.5 %), and C_{60}-based LB film cells (1.2-8.2 %). The value obtained here is smaller than that of the mixed SAMs (as high as 50±8 % in quantum yield) reported by Imahori *et al.*[9c], but ferrocene-porphyrin-C_{60} triad and boron-dipyrrin light-harvesting molecule were used in that system.

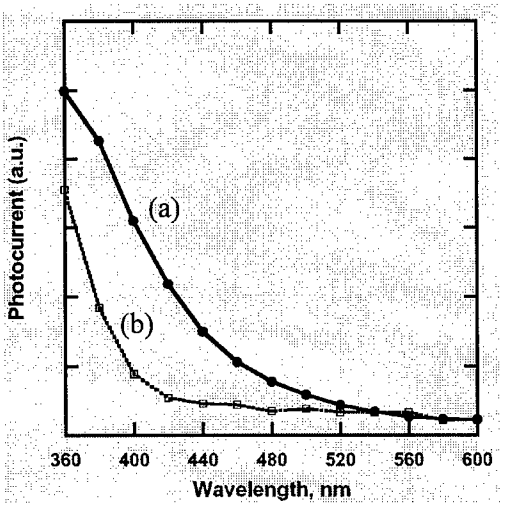

Figure 12. (a) Action spectrum of mixed SAM and (b) UV/vis spectrum of mixed solution with the feeding molar ratio of 10:1 (**2**:**1**) (in toluene); electrolyte solution: 0.1 M Na_2SO_4 solution containing 50 mM methyl viologen (MV^{2+}) as an electron carrier; input power: 0.85 W/cm^2; applied potential: -100 mV vs Ag/AgCl.

This result encouraged us to employ a very electron-deficient C_{60}-MPAA as electron acceptor to further improve the efficiency of ET. Even higher photocurrent generation (1,700 nA cm^{-2}) was achieved with a molar ratio (10:1) of D/A co-assembled on the substrate. We also learned that the photocurrent intensity varies significantly with changes in D/A ratio. This is because similar conjugating molecules tend to form aggregates during the self-assembly process, thus creating multiple isolated D/A domains in the SAM. This kind of morphology does not favour efficient ET because of the positional and functional irregularity (Figure 13). We could therefore harness the full potential of photocurrent generation by controlling the organization of D/A domains in nanoscale.

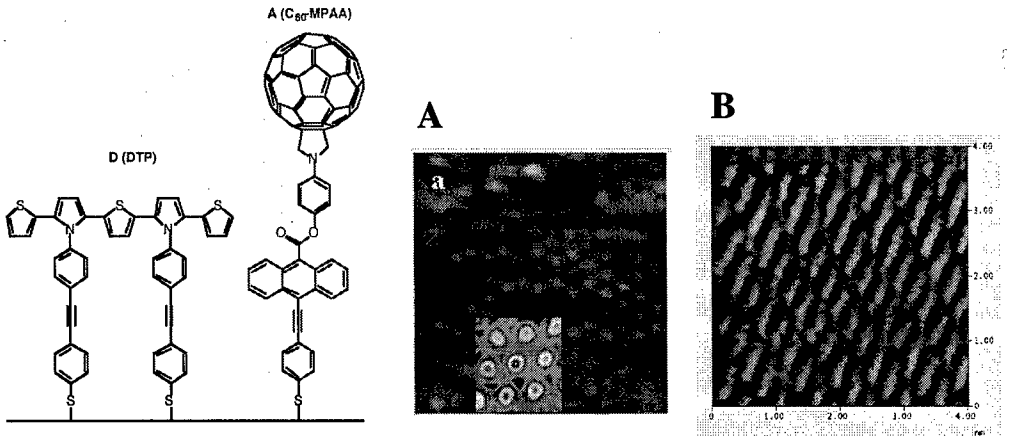

Figure 5. STM images of SAMs from (A) the assembly of C_{60}-MPAA itself and (B) the coassembly of DTP and C_{60}-MPAA (10:1 of molar ratio).

The quantum efficiency (Φ) of charge separation from D to A is close to unity in the system with C_{60} as electron acceptor because the time scale for photoinduced ET is sub-picosecond, more than 10^3 times faster than the radiative or nonradiative decay of photoexcitations. In principle, we could construct an ideal molecular light-to-current converter if we could only engineer a monolayer device where the donors and acceptors are organized in alternating arrays that are spaced within the exciton diffusion length (~10 nm) from each other. It is nearly impossible to precisely control the co-assembly of D and A molecules to produce well-distributed D/A domains of desired sizes because the resulting structure is determined by the interplay of kinetics and thermodynamics of the self-assembly process. Thus, in our forthcoming work, a highly efficient photocurrent generation system made of a well-distributed network of D/A arrays will be built by selective binding electron donor/acceptor functional systems onto two-dimensional nanostructure created with proteins as molecular templates.

Personnel

Principal Investigator: A. K-Y. Jen
Co-PI: Mehmet Sarikaya
Mailing Address: Department of Materials Science and Engineering, University of Washington, Seattle, WA 98195-2120
Phone Number: 206-543-2626
Fax Number: 206-543-3100
E-mail address: ajen@u.washington.edu

- Total number of Full-Time equivalent Graduate Students and Post-doctoral Associates supported during this period under F49620-97-1-0541

  Graduate Students: 1.5
  Postdoctoral Associate: 0.5
  including number of

Female graduate students: 1
Female Post-doctoral Associates: 0
Minority* graduate students: 0
Minority* Postdoctoral Associates: 0
Asian Graduate Students: 1.5
Asian Postdoctoral Associates: 0.5

- **Publications**

a. Number of papers submitted to referred Journals, but not published: 3
b. +Numbers of papers published in refereed journals (for each, please provide a complete citation): 6
c. +Number of books or chapters submitted, but not yet published: 1
d. +Number of books or chapters published (for each, provide a complete citation): 0
e. +Number of printed technical reports/non-refereed papers (for each, provide a complete citation): 0
f. +Number of patents filed: 0
g. +Number of patents granted (for each, provide a complete citation): 0
h. +Number of invited presentations (for each, provide a complete citation): 8
i. +Number of submitted presentations (for each, provide a complete citation): ?
j. +Honors/Awards/Prizes for contract/grant employees: ?

a) Papers submitted to refereed journals:

1. "Efficient Photocurrent Generation through a Self-assembled Monolayer of C_{60}-Phenylacetylene-anthryl with Ordered Structure", Kang, M.-S.; Kang, S. H.; Ma, H.; Kim, K.-S.; Jen, A. K.-Y. *Langmuir.*, (submitted).
2. "Self-Assembly of Aromatic-Derivatized Thiols under Various Intermolecular Interaction Schemes ", R. F. Dou, Y. S. Yang, X-C. Ma, J. F. Jia, Q. K. Xue, L. Xi, H.C. Ong, K. Y. Wong, W. M. Lau, H. Ma, H. L. Yip, A. K-Y Jen, , and J. Am. Chem. Soc., (submitted).
3. "Synthetic and Biomimetic Molecular Erectors", M. Sarikaya, C. Tamerler, H. Zareie, H. Ma, A. K-Y. Jen, *Polymer*, (in press).

b) Papers published in refereed journals

1. "Ordered Self-Assembly and Electronic Behavior of C_{60}-anthrylphenylacetylene Hybrid", Kang, S. H.; Ma, H.; Kang, M.-S.; Kim, K. -S.; Jen, A. K.-Y.; Zareie, M. H.; Sarikaya, M. *Angew. Chem. Int. Ed.* **2004**, *43*, 1512.
2. "Highly Efficient Photocurrent Generation from a Self-Assembled Monolayer Film of a Novel C_{60}-Tethered 2,5-Dithienylpyrrole Triad", Kim, K. S.; Kang, M. S.; Ma, H.; Jen, A. K.-Y. *Chem. Mater.* **2004,** *16(24)*, 5058.
3. "Functional Self-assemblies for Photocurrent Generation", H. Ma and A. K-Y. Jen, an Invited Article to Spectrum, **2004**, *17(3)*, 24.
4. "Thiol-Linked Anthraquinone Anthryl Acetylene Molecule: Synthesis, Ordered Self-Assembly, and Photoelectrochemical Properties", H. Ma, M. S. Kang, Q. M. Xu, K. S. Kim, and A. K.-Y. Jen, Chem. Mater., **2005**, *17*, 2896.

5. "The Assembly of Terphenyl- and Quaterphenyl-dithiol on Gold and Gallium Arsenide: Solvent Effects: Investigated by NEXAFS", D. Krapchetov, H. Ma, A. K-Y. Jen, D. A. Fischer, and Y-L. Loo, Langmuir, **2005**, *21*, 5887.
6. "Assembly of Gold Nanoparticles Using Genetically Engineered Polypeptides", M. Zin, H. Ma, M. Sarikaya, A. K-Y. Jen, Small, **2005**, *1(7)*, 698.

h) Invited presentations

1. "Nanoscale Tailoring of Organic Functional Materials for Photonics and Molecular Electronics", Alex Jen, Department of Chemistry, University of Texas, Austin, TX, 3/04.
2. "Nanoscale Tailoring of Organic Functional Materials for Photonics and Molecular Electronics", Alex Jen, National Tsing Hus University, Hsin Chu, Taiwan, 3/04.
3. "Nanoscale Tailoring of Organic Functional Materials for Photonics and Molecular Electronics", Alex Jen, Macro 2004, Paris, France, 7/04.
4. "Nanoscale Architectural Control of Organic Functional Materials for Photonics and Molecular Electronics", Alex Jen, SPIE Meeting, Denver, 8/04.
5. "Nanoscale Architectural Control of Organic Functional Materials for Photonics and Molecular Electronics", Alex Jen, ACS Meeting, Philadelphia, 8/04.
6. "Controlled Self-Assembly of Fused-Ring Aromatics for Molecular Electronics and Photocurrent Generation", Alex Jen, MRS Meeting, San Francisco, 4/04.
7. "Exceptional Photonic and Optoelectronic Properties through Molecular Design and Controlled Self-Assembly", Material Research Society Meeting, San Francisco, 4/05.
8. "Exceptional Photonic and Optoelectronic Properties through Molecular Design and Controlled Self-Assembly", University of California, Davis, 12/04.
9. "Exceptional Photonic and Optoelectronic Properties through Molecular Design and Controlled Self-Assembly", Rutgers University, New Jersey, 1/05.

c) Transition

We have been working with Professor Lynn Loo from the University of Texas, Austin to use nano-transfer printing technique to print our molecular wires on semiconductor surface (GaAs) for measuring both molecular conductance and metal/organic interfacial behavior. We are also working with Professor Francesco Stellachi (MIT) to functionalize our molecular wires on Au nanoparicles.